Gold Nanocages: Bioconjugation and Their Potential Use as Optical Imaging Contrast Agents

ARTICLE *in* NANO LETTERS · MARCH 2005

Impact Factor: 13.59 · DOI: 10.1021/nl047950t · Source: PubMed

NANO LETTERS

2005
Vol. 5, No. 3
473−477

Gold Nanocages: Bioconjugation and Their Potential Use as Optical Imaging Contrast Agents

Jingyi Chen,[†,+] Fusayo Saeki,[‡,+] Benjamin J. Wiley,[§] Hu Cang,[†,‡] Michael J. Cobb,[‡] Zhi-Yuan Li,[||] Leslie Au,[†] Hui Zhang,[⊥] Michael B. Kimmey,[#] Xingde Li,*[,‡] and Younan Xia*[,†]

Department of Chemistry, Department of Bioengineering, Department of Chemical Engineering, Division of Gastroenterology, Department of Medicine, University of Washington, Seattle, Washington 98195, Institute of Physics, Chinese Academy of Sciences, Beijing 10080, China, and Institute for Systems Biology, Seattle, Washington 98103

Received December 10, 2004; Revised Manuscript Received January 26, 2005

ABSTRACT

Gold nanocages of <40 nm in dimension have been synthesized using the galvanic replacement reaction between Ag nanocubes and $HAuCl_4$ in an aqueous solution. By controlling the molar ratio between Ag and $HAuCl_4$, the gold nanocages could be tuned to display surface plasmon resonance peaks around 800 nm, a wavelength commonly used in optical coherence tomography (OCT) imaging. OCT measurements on phantom samples indicate that these gold nanocages have a moderate scattering cross-section of $\sim 8.10 \times 10^{-16}$ m^2 but a very large absorption cross-section of $\sim 7.26 \times 10^{-15}$ m^2, suggesting their potential use as a new class of contrast agents for optical imaging. When bioconjugated with antibodies, the gold nanocages have also been demonstrated for specific targeting of breast cancer cells.

Optical coherence tomography (OCT) has emerged as a promising biomedical diagnostic tool for noninvasive, in situ imaging of biological tissues and materials.[1] Since the image contrast mainly comes from the scattering and absorption of light by tissues, both the sensitivity and specificity of OCT have a strong dependence on the intrinsic optical properties of the biological sample. Recently, several types of contrast agents based on optical scattering or absorption have been demonstrated for optical imaging, including OCT and photoacoustic tomography.[2] Gold nanoparticles are particularly attractive for OCT contrast enhancement because their optical resonance wavelengths can be precisely tuned over a broad range by controlling their sizes and shapes (among other parameters).[3] In addition, some new types of nanoparticles with specially designed structures can strongly absorb near-infrared radiation and provide thermal therapeutic treatment by elevating the temperature of targeted tissues.[4] We have recently demonstrated the synthesis of gold nanocages (hollow nanostructures with porous walls) through the galvanic replacement reaction between silver templates and chloroauric acid.[5] Different from previously reported nanostructures (such as Au shells and SiO_2@Au core−shell colloids),[6] our nanocages could be prepared with much smaller dimensions (on the scale of 40 nm) while maintaining strong optical resonance peaks in the near-IR region (800−1200 nm). We further demonstrate that these gold nanocages could be conveniently functionalized with tumor-specific antibodies, and serve as a new class of contrast agents for OCT.

Figure 1A shows SEM and TEM images of silver nanocubes that were synthesized using a polymer-mediated polyol process.[7] By optimizing the experimental conditions, the dimensions of these nanocubes could be readily controlled below 30 nm.[8] Figure 1B shows SEM and TEM images of a typical sample of gold nanocages, which has an extinction peak around 800 nm (see Figure 2A). Synthesis of these nanocages was conducted following the procedure described in our previous publications.[5] In a typical procedure, 5 mg poly(vinyl pyrridone) (Aldrich, M. W. $\approx$ 10,000) was added to 5 mL of deionized water and heated to boiling before a 75-μL aliquot of a silver nanocube dispersion (8.1 mM in terms of silver) was added to the solution. This diluted dispersion of silver nanocubes was then refluxed for 2 min

* Corresponding authors. E-mail: xia@chem.washington.edu and xingde@u.washington.edu.
[†] Department of Chemistry, University of Washington.
[‡] Department of Bioengineering, University of Washington.
[§] Department of Chemical Engineering, University of Washington.
[#] Department of Medicine, University of Washington.
[||] Chinese Academy of Sciences.
[⊥] Institute for Systems Biology.
[+] These two authors contributed equally to this work.

10.1021/nl047950t CCC: $30.25
Published on Web 02/08/2005

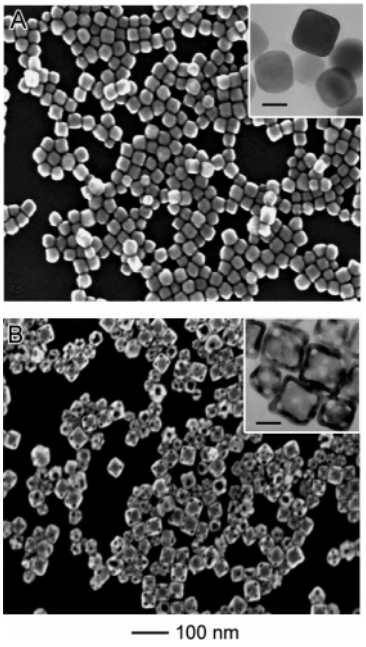

Figure 1. (A) SEM image of the as-synthesized silver nanocubes with edge lengths on the scale of 30 nm. (B) SEM image of gold nanocages (nanoboxes with truncated corners) prepared by refluxing an aqueous solution containing both silver nanocubes and $HAuCl_4$. The insets show TEM images of these nanocubes and nanocages, with the scale bars representing 20 nm.

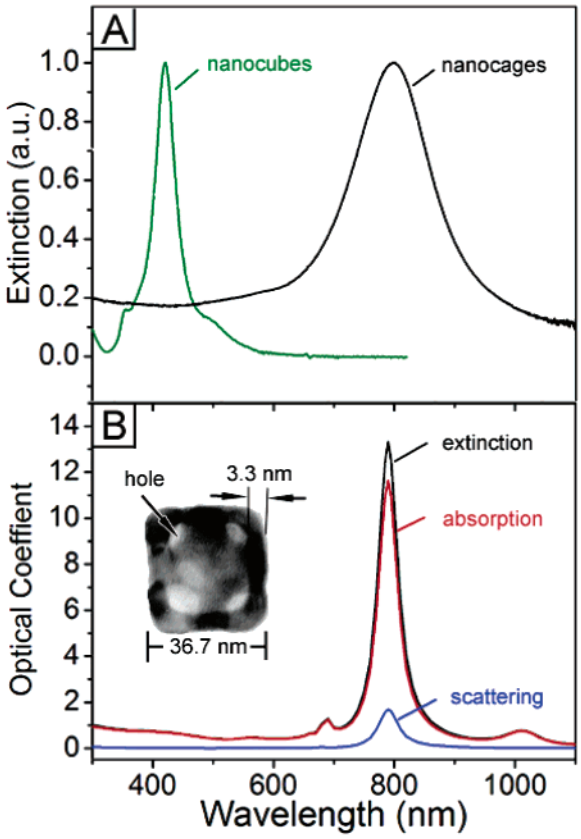

Figure 2. (A) UV−vis−near-IR extinction spectra recorded from aqueous suspensions of silver nanocubes and gold nanocages (shown in Figure 1), respectively. (B) Extinction, scattering, and absorption coefficients ($Q = C/\pi a_{eff}^2$) calculated for a gold nanocage with the pore structure and dimensions illustrated by the TEM image in the inset (see the text for detail).

before 750 μL of 0.2 mM $HAuCl_4$ aqueous solution was added using a microsyringe pump at a rate of 0.8 mL/min. The solution was refluxed for another 10 min until its color became stable. Vigorous magnetic stirring was applied in the entire process. After the solution had been cooled to room temperature, a white AgCl precipitate formed, and this was dissolved by adding a saturated solution of NaCl. The mixture was then centrifuged at 10,000 rpm for 15 min, and the supernatant containing the dissolved AgCl was decanted. The product was then rinsed with water and centrifuged for two more times, and finally re-dispersed in water for further usage. As shown by the SEM and TEM images, each nanocage had small holes at their corners and (possibly) side faces. The edge length and wall thickness of these nanocages (calculated from 50 nanocages based on their TEM images), 36.7 ± 3.5 and 3.3 ± 0.2 nm, respectively, were close to the values estimated from the stoichiometry for the replacement reaction (i.e., oxidation of every three Ag atoms only generates one Au atom). It is worth pointing out that such hollow and porous nanostructures composed of very thin walls were mechanically robust enough to sustain their shapes during the preparation of SEM and TEM samples, which typically involves strong capillary forces as the solvent evaporates.[9]

Similar to silver nanocubes larger than 100 nm in dimension, the surface plasmon resonance peak was continuously shifted from the visible to the near-IR when the 30-nm silver nanocubes were transformed into gold nanocages with different void/pore sizes. In practice, the resonance peak could be tuned to any specific wavelength in the spectral range from 400 to 1000 nm by titrating a specific amount of aqueous suspension of silver nanocubes with different amounts of an aqueous $HAuCl_4$ solution. Figure 2A shows the extinction spectra obtained from an aqueous suspension of silver nanocubes and gold nanocages, respectively. Both of the spectra have been normalized to their peak intensities. Figure 2B shows the extinction (Q_{ext}), absorption (Q_{abs}), and scattering (Q_{sca}) coefficients (note that $Q_{ext} = Q_{abs} + Q_{sca}$) of a gold nanocage computed using the discrete dipole approximation (DDA) method.[10] As illustrated in the inset, the nanocage was assumed to have a cubic shape with an edge length of 36.7 nm and a wall thickness of 3.3 nm. All of the corners were truncated to create eight triangular holes of 5 nm in base dimension. In calculation, the cage was divided into an array of N consecutive cells, with each cell being approximated as a polarizable point electric dipole with a moment $\mathbf{P}_i$. Under the excitation of a monochromatic optical field, these dipoles oscillate, couple with each other, and reradiate light. The refractive index of bulk gold was used, and the nanocage was assumed to be surrounded and filled by water. Both absorption and scattering cross-sections (C_{abs} and C_{sca}) could be directly obtained from $\mathbf{P}_i$. In plotting the spectra, the cross-sections were divided by πa_{eff}^2 (with a_{eff} being defined through the concept of an effective volume equal to $4\pi a_{eff}^3/3$ for the nanocage) to obtain the dimensionless coefficients (Q). The calculated curves match well with the experimentally measured spectrum. The discrepancy in the peak width could be attributed to the fact that the

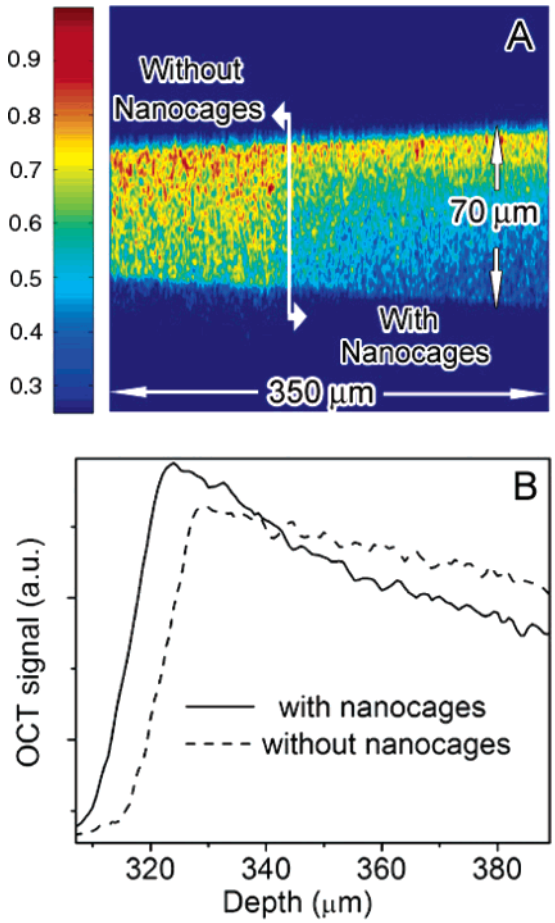

Figure 3. (A) OCT image of a gelatin phantom embedded with TiO_2, and the concentration of TiO_2 was controlled at 1 mg/mL to mimic the background scattering of soft tissues. The right portion of the phantom contained 1 nM of gold nanocages while the left portion did not contain any gold nanocages. (B) Plots of the OCT signals on a log scale as a function of depth. Note that the OCT signal recorded from the portion of phantom with gold nanocages decays faster than the portion without nanocages.

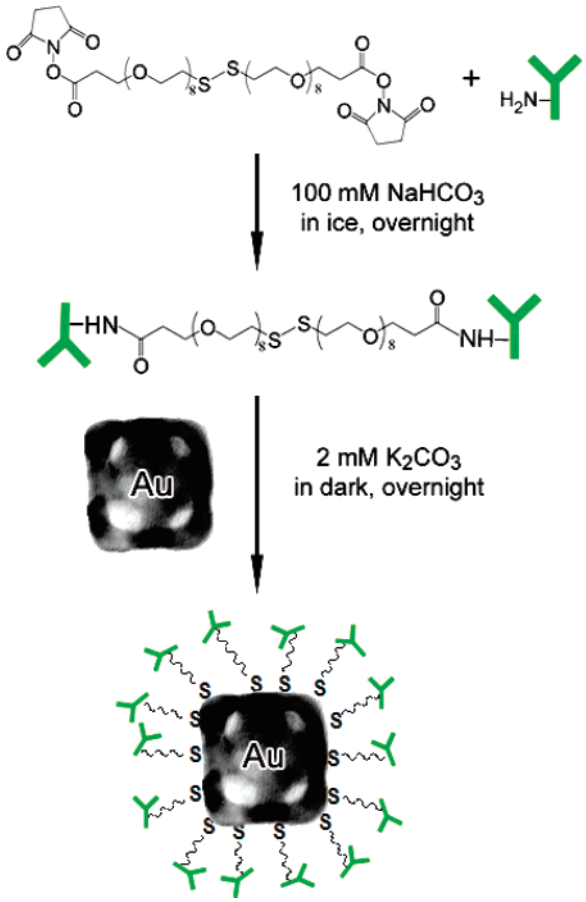

Figure 4. A schematic illustration of the two-step protocol used to conjugate antibodies to the surface of a gold nanocage. In the first step, succinimidyl propionyl poly(ethylene glycol) disulfide (NHS-activated PEG, M.W. = 1,109) was reacted with the primary amine of an antibody. In the second step, the PEG−antibody complex was bonded to the gold nanocage (as represented with a TEM image) by breaking its internal disulfide bond and forming a Au−S linkage.

nanocages in a real sample might have a distribution in size and wall thickness, as well as different degrees of corner truncation. Because of their small sizes and thin walls, these gold nanocages are expected to be most effective in absorbing rather than scattering the incident light. On the basis of our DDA calculation, the C_{abs} and C_{sca} were found to be 7.63×10^{-15} m^2 and 1.10×10^{-15} m^2, respectively, and the ratio of C_{abs} to C_{sca} was 6.92 for the gold nanocage depicted in Figure 2B.

To demonstrate the potential of gold nanocages as a class of contrast agents, OCT imaging was performed on phantom samples with and without nanocages. The phantom was made of gelatin embedded with TiO_2 granules to mimic the scattering background in biological samples. OCT imaging was conducted using a 7-fs Ti:sapphire laser with a center wavelength at 825 nm and a bandwidth of 155 nm. The measured axial resolution in air and detection sensitivity of this system were ~2.7 μm and ~−104 dB, respectively. In Figure 3A, the left portion of the OCT image corresponds to the sample without nanocages, and the right portion corresponds to the sample with nanocages. The log of the OCT signal as a function of depth is plotted in Figure 3B. The presence of gold nanocages increases the rate of decay significantly. By fitting the decay curve to an analytic expression that describes the OCT axial scan,[11] we could obtain both the scattering and extinction cross-sections (C_{sca} and C_{ext}) of a sample. For the sample with gold nanocages, C_{sca} and C_{ext} obtained from curve fitting are the sum of contributions from TiO_2 particles and Au nanocages. Since the TiO_2 particles have negligible absorption at 800 nm, the extinction cross-section measured from the sample without nanocages is then assumed to be the same as the scattering cross-section of TiO_2. When the scattering of TiO_2 was subtracted, we estimated that the scattering cross-section (C_{sca}) of a gold nanocage was 8.10×10^{-16} m^2 while the absorption cross-section (C_{abs}) was on the order of 7.26×10^{-15} m^2. The ratio between the absorption and scattering cross-sections was 8.97, which was close to the value (6.92) derived from the calculated spectra shown in Figure 2B. Compared with the conventional dye Indocyanine Green (ICG),[12] which has an absorption cross-section of 2.90×10^{-20} m^2 at 800 nm, the absorption of these gold nanocages is about 5 orders of magnitude stronger. These results imply

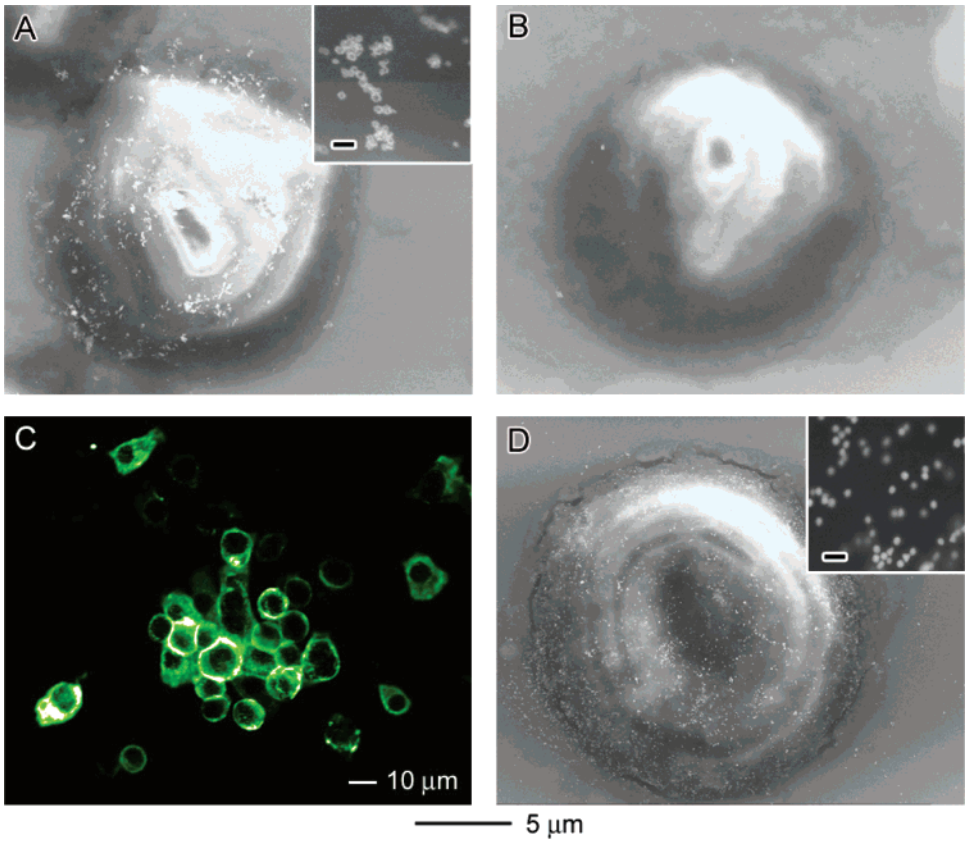

Figure 5. (A) SEM image of an SK-BR-3 cancer cell whose surface was derivatized with the primary anti-HER2 antibodies and then the IgG-conjugated gold nanocages. The inset shows an SEM image at higher magnification, indicating that the nanocages were dispersed as a single layer on the cell surface. (B) SEM image of a control where cancel cells without the primary anti-HER2 on their surfaces were incubated with gold nanocages. (C) Fluorescence image of SK-BR-3 cells whose surfaces were treated with the anti-HER2 antibodies, followed by incubation with FITC−IgG. The uniform green color implies a relatively homogeneous distribution of the primary anti-HER2 antibodies on the cell surface. (D) SEM image of a SK-BR-3 cancer cell that was derivatized using the same protocol as in (A) except the substitution of gold nanocages with commercial gold nanoparticles. The scale bars in the inset represent 100 nm.

that gold nanocages represent a new class of absorption contrast agents for OCT imaging. The extremely large absorption cross-sections also suggest their use as a potential thermal therapeutic agent.

Gold nanocages were also functionalized with biological molecules to target cancer cells for early-stage diagnostics and thermal therapy of tumors. A breast cancer cell line, SK-BR-3, which overexpresses epidermal growth factor receptor 2 (EGFR2 or HER2), was used to test the molecular specific binding of bioconjugated gold nanocages.[13] In a typical procedure, primary antibodies (monoclonal anti-HER2 antibody from mouse) were first immobilized on the cancer cells by incubating the SK-BR-3 cells in a buffer containing anti-HER2 antibodies. Excess anti-HER2 antibodies were removed by washing the cells with Tris-buffered saline Tween-20 (TBST). Gold nanocages were conjugated with a secondary antibody (e.g., anti-mouse immunoglobulin G or IgG), following the protocol shown in Figure 4. In the final step, a buffer solution containing IgG-conjugated nanocages was applied to SK-BR-3 cells bound with anti-HER2 antibodies. Figure 5A shows the distribution of gold nanocages on the surface of SK-BR-3 cells as revealed by scanning electron microscopy (SEM). Three control experiments were also conducted to further support our findings. First, SK−BR-3 cells without the primary anti-HER2 on their surfaces were incubated with the gold nanocages, and the result is shown in Figure 5B. It is clear that essentially no gold nanocages could be observed on the cell surface. Second, SK-BR-3 cells were derivatized with the anti-HER2 antibodies, followed by incubation with FITC-labeled IgG. Figure 5C shows a fluorescence image of the cells. The uniform green color implies a relatively homogeneous distribution of the primary anti-HER2 antibody on the cell surface. Finally, SK-BR-3 cancer cells were treated with the same protocol as in Figure 5A except the substitution of gold nanocages with commercial gold nanoparticles (∼40 nm in diameter, Ted Pella, Redding, CA). It is clear that our gold nanocages behave similarly when compared with conventional gold colloids that have already found widespread use as bio-markers.[14] The results of these studies clearly establish that the bioconjugated gold nanocages can serve as a molecular probe to target the desired cancer cells. The density of nanocages immobilized on the surface of a cell depends on the concentration of the nanocages and will be optimized in the future work.

In summary, gold nanocages of <40 nm in dimension have been synthesized, and their surface plasmon resonance peaks were readily tuned to the specific wavelength (∼800 nm) required for OCT imaging. Our preliminary OCT imaging results indicate that gold nanocages strongly absorb light in

the near-IR region, with an absorption cross-section 5 orders of magnitude higher than the most commonly used organic dyes such as ICG. We have further bioconjugated gold nanocages to specifically bind to the surfaces of cancer cells. The present work suggests that gold nanocages are promising as both a contrast agent for optical diagnostics of cancers and as a potential thermal therapeutic agent for cancer treatment.

We note that micrometer-sized polymer beads and SiO_2/Au nanoshells have already been demonstrated for such applications.[2−4] The gold nanocages described here will provide, at least, four major advantages over previous systems: (i) their surface plasmon resonance peaks can be conveniently tuned to cover the entire spectral region from 500 to 1200 nm by simple controlling the experimental parameters (e.g., the molar ratio between Ag nanocubes and $HAuCl_4$); (ii) their scattering and absorption coefficients can be easily varied by changing the void sizes and number of truncated corners; (iii) the gold nanocages can be made extremely small (<50 nm) while still exhibiting resonance peaks in the near-IR region; and (iv) their surfaces can be readily derivatized with various functional groups by taking advantage of the well-established thiolate monolayer chemistry.

Acknowledgment. This work was supported in part by a Fellowship from the David and Lucile Packard Foundation, an Alfred P. Sloan Research Fellowship, and a Camille Dreyfus Teacher Scholar Award (to Y.X.); as well as the NIH, the Whitaker Foundation, and the NSF CAREER Award (to X.L.). J.C. and B.W. thank the Center for Nanotechnology at the UW for a Nanotech Student Fellowship Award and an IGERT Fellowship Award (supported by the NSF, DGE−9987620), respectively. F.S. and M.C. acknowledge their fellowships from the NIH GI and Oral Biology Training Grants. L.A. thanks the Mary Gates Endowment for Students at the UW for a Research Training Grant. We are grateful to Dr. Mon Thiri Myaing and Mr. Daniel MacDonald for their assistance with the OCT phantom imaging. The SEM work was performed at the Nanotech User Facility (NTUF), a member of the National Nanotechnology Infrastructure Network (NNIN) funded by the NSF.

References

(1) Huang, D.; Swanson, E. A.; Lin, C. P.; Schuman, J. S.; Stinson, W. G.; Chang, W.; Hee, M. R.; Flotte, T.; Gregory, K.; Puliafito, C. A.; Fujimoto, J. G. *Science* **1991**, *254*, 1178.

(2) See, for example, (a) Lee, T. M.; Oldenburg, A. L.; Sitafalwalla, S.; Marks, D. L.; Luo, W.; Toublan, F. J.; Suslick, K. S.; Boppart, S. A. *Opt. Lett.* **2003**, *28*, 1546. (b) Xu, C. Y.; Ye, J.; Marks, D. L.; Boppart, S. A. *Opt. Lett.* **2004**, *29*, 1647. (c) Yang, C.; Choma, M. A.; Lamb, L. E.; Simon, J. D.; Izatt, J. A. *Opt. Lett.* **2004**, *29*, 1396. (d) Wang, R. K.; Elder, J. B. *Lasers in Surgery & Medicine* **2002**, *30*, 201. (e) Yang, C.; McGukin, L. E. L.; Simon, J. D.; Choma, M. A.; Applegate, B. E.; Izatt, J. A. *Opt. Lett.* **2004**, *29*, 2016.

(3) (a) Loo, C.; Lin, A.; Hirsch, L.; Lee, M. H.; Barton, J.; Halas, N.; West, J.; Drezek, R. *Technol. Cancer Res. Treat.* **2004**, *3*, 33. (b) Wang, Y.; Xie, X.; Wang, X.; Ku, G.; Gill, K. L.; O'Neal, D. P.; Stoica, G.; Wang, L. V. *Nano Lett.* **2004**, *4*, 1689. (c) Copland, J. A.; Eghtedari, M.; Popov, V. L.; Kotov, N.; Mamedova, N.; Motamedi, M.; Oraevsky, A. A. *Mol. Imaging Biol.* **2004**, *6*, 341. (d) Sokolov, K.; Follen, M.; Aaron, J.; Pavlova, I.; Malpica, A.; Lotan, R.; Richards-Kortum, R. *Cancer Res.* **2003**, *63*, 1999. (e) Chen, K.; Liu, Y.; Ameer G.; Backman, V. *J. Biomecical Opt.* **2005**, *10*, in press.

(4) Hirsch, L. R.; Stafford, R. J.; Bankson, J. A.; Sershen, S. R.; Rivera, B.; Price, R. E.; Hazle, J. D.; Halas, N. J.; West, J. L. *Proc. Natl. Acad. Sci. U.S.A.* **2003**, *100*, 13549.

(5) (a) Sun, Y.; Xia, Y. *J. Am. Chem. Soc.* **2004**, *126*, 3892. (b) Sun, Y.; Mayers, B. T.; Xia, Y. *Adv. Mater.* **2003**, *15*, 641. (c) Sun, Y.; Xia, Y. *Nano Lett.* **2003**, *3*, 1569.

(6) (a) Oldenburg, S. J.; Averitt, R. D.; Westcott, S. L.; Halas, N. J. *Chem. Phys. Lett.* **1998**, *288*, 243. (b) West, J. L.; Halas, N. J. *Annu. Rev. Biomed. Eng.* **2003**, *5*, 285.

(7) (a) Wiley, B.; Sun, Y.; Mayers, B.; Xia, Y. *Chem. Eur. J.* **2005**, *11*, 454. (b) Wiley, B.; Herricks, T.; Sun, Y. and Xia, Y. *Nano Lett.* **2004**, *4*, 1733.

(8) For the nanocube synthesis, 5 mL ethylene glycol (EG, J. T. Baker, 9300−01) was first heated at 149 °C for 8 min under a 0.5 SLPM flow of nitrogen. This was done to quickly remove water. Heating was continued under air for another 52 min. A syringe pump (KDS-200, Stoelting, Wood Dale, IL) then regulated the simultaneous injection of two 3-mL EG solutions into the hot EG at a rate of 45 mL per hour. One of the solutions contained 94 mM silver nitrate (Aldrich, 209139−100G), and the other contained 144 mM poly(vinyl pyrrolidone) (PVP, M. W.≈55,000, Aldrich, 856568−100G, the concentration was calculated in terms of the repeating unit), and 0.22 mM NaCl (Fisher, S271−500). Magnetic stirring was applied throughout the synthesis. The solution typically turned yellow, orange, and then clear within the first hour after injection. After ~20 h, the solution became orange-red, indicating the presence of 30-nm silver cubes. At this time the reaction was stopped and the nanocubes were washed with acetone and then water before being dispersed in water for galvanic replacement reaction.

(9) Korgel, B. A.; Fitzmaurice, D. *Adv. Mater.* **1998**, *10*, 661.

(10) (a) Draine, B. T.; Flatau, P. J. *J. Opt. Soc. Am. A* **1994**, *11*, 1481. (b) Li, Z. Y.; Gu, B. Y.; Yang, G. Z. *Phys. Rev. B* **1997**, *57*, 10883. (c) Sosa, I. O.; Noguez, C.; Barrera, R. G. *J. Phys. Chem. B* **2003**, *107*, 6269. (d) Jin, R.; Cao, Y.; Mirkin, C. A.; Kelly, K. L.; Schatz, G.; Zheng, J.-G. *Science* **2001**, *107*, 668.

(11) Schmitt, J. M.; Knuttel, A.; Bonner, R. F. *Appl. Opt.* **1993**, *32*, 6032.

(12) Carski, T. R. *An Investigator's Brochure, "Indocyanine Green: History Chemistry Pharmacology Indiction Adverse Reactions Investigation and Prognosis"*; Becton Dickinson and Company: Hunt Valley, MD, June 24, 1994.

(13) (a) Yarden, Y.; Sliwkowski, M. X. *Nature* **2001**, *2*, 127. (b) Molina, M. A.; Codony-Servat J.; Albanell, J.; Rojo, F.; Arribas, J.; Basela, *J. Cancer Res.* **2001**, *61*, 4744.

(14) Hayat, M. A. *Colloidal Gold: Principles, Methods and Applications*, Academic Press: San Diego, CA, 1989.

NL047950T